Photoelectrochemical activity of CdS/Ag/TiO_2 nanorod composites: Degradation of nitrobenzene coupled with the concomitant production of molecular hydrogen

Yi Zhang, Chenchen Yuan, Qiang Wang, Michael R. Hoffmann, Xingwang Zhang, Jutao Nie, Chao Hu, Shuxin Chen, Jie Qiao, Qi Wang, Yanqing Cong

PII: S0013-4686(19)31995-4

DOI: https://doi.org/10.1016/j.electacta.2019.135124

Reference: EA 135124

To appear in: *Electrochimica Acta*

Received Date: 22 August 2019

Revised Date: 14 October 2019

Accepted Date: 19 October 2019

Please cite this article as: Y. Zhang, C. Yuan, Q. Wang, M.R. Hoffmann, X. Zhang, J. Nie, C. Hu, S. Chen, J. Qiao, Q. Wang, Y. Cong, Photoelectrochemical activity of CdS/Ag/TiO_2 nanorod composites: Degradation of nitrobenzene coupled with the concomitant production of molecular hydrogen, *Electrochimica Acta* (2019), doi: https://doi.org/10.1016/j.electacta.2019.135124.

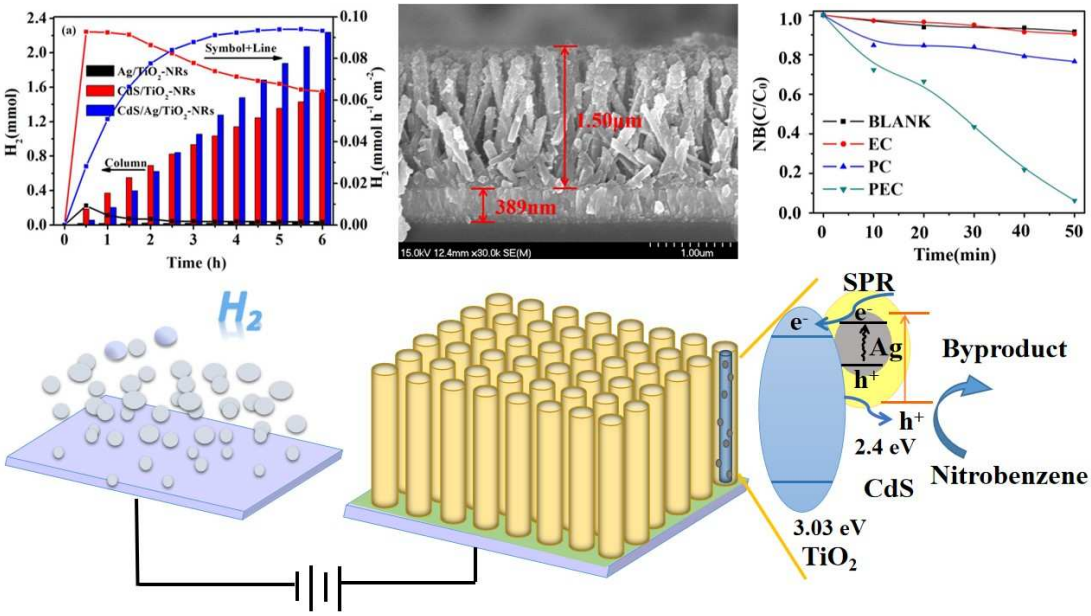

Photoelectrochemical Activity of CdS/Ag/TiO_2 Nanorod Composites: Degradation of Nitrobenzene Coupled with the Concomitant Production of Molecular Hydrogen

Yi Zhang[a,b*], Chenchen Yuan[a], Qiang Wang[a], Michael R. Hoffmann[b], Xingwang Zhang[c], Jutao Nie[a], Chao Hu[a], Shuxin Chen[a], Jie Qiao[a], Qi Wang[a], Yanqing Cong[a]

[a] *School of Environmental Science and Engineering, Zhejiang Gongshang University, Hangzhou 310018, China*

[b] *Linde-Robinson Laboratories, California Institute of Technology, Pasadena, CA 91125, USA*

[c] *Key Laboratory of Biomass Chemical Engineering of Ministry of Education, College of Chemical and Biological Engineering, Zhejiang University, Hangzhou, Zhejiang, 310027, China*

Abstract

TiO_2 nanorods decorated with CdS and Ag^0 were prepared and anchored on to a fluorine doped tin oxide (FTO) electrode in order to investigate the photoelectrochemical (PEC) oxidation of nitrobenzene coupled with simultaneous reduction of water to produce molecular hydrogen. The modified TiO_2 nanorods (TiO_2-NRs) prepared for 4 h have regular nanoroads with high superficial area and Ag particles loaded on the surface of nanoroads covered with CdS film uniformly. The nano-composite TiO_2-NRs with photochemically active up to 700 nm with coupled photoconversion efficiencies for nitrobenzene (NB) degradation and hydrogen (H_2) production as high as 4.4%. The surface plasmon resonance (SPR) effect of Ag not only excited the photo-generated electron of Ag nanoparticles, but also promoted the electron transfer from

*To whom correspondence should be addressed. E-mail: zhangyi@zjgsu.edu.cn.

CdS to TiO_2-NRs. NB as a role of electron donor, reacts with hole to improve the efficiency of H_2 production. The heterostructure electrode for solar energy conversion had an important significance for solving environmental pollution and energy crisis.

Keywords: Photoelectrochemical Catalysis; Cadmium Sulfide; Elemental Silver; Surface Plasmonic Resonance; Nitrobenzene and Hydrogen

1. Introduction

Molecular hydrogen (H_2) is produced commercially primarily by water electrolysis [1], methanol or ammonia decomposition [2], and natural-gas steam reformation [3]. However, the cost of production in terms of actual environmental impacts can be quite high. Photocatalytic (PC), electrochemical (EC) and photoelectrochemical (PEC) production of H_2 has been the focus of much research over the past 30 years [4-6]. The major challenge remains the search for low-cost, earth-abundant semiconducting materials that are stable under a broad range of pH conditions (e.g., 1 M H_2SO_4 to 1 M NaOH) and are photo-active through-out the prime regions of the incident solar spectrum.

In 1921, Baur and Rebmann [7] reported that semiconductor composites of thalium chloride (E_g = 3.8 eV) and AgCl (E_g = 3.3 eV) could be used for the stoichiometric splitting of water upon absorption of wavelengths of UV light < 370 nm. Baur and Rebmann showed that an illuminated mixture of TlCl/AgCl semiconductors suspended in water could achieve stoichiometric photochemical water splitting in a 2:1 mole ratio of H_2 to O_2. Fifty years later, Fujishima and Honda [8] used a single-crystal of rutile (TiO_2) photoanode (E_g = 3.0 eV) coupled with a platinum black cathode to demonstrate PEC water splitting at pH 4.7 in an acetic acid/acetate buffer system mixed into a 0.5 M KCl/KI background electrolyte. The anodic and cathodic chambers were separated by sintered glass diagram or glass frit. During the intervening 46 years much research has been undertaken to advance our understanding of both pure homogeneous and heterogeneous water splitting (i.e., no sacrificial electron donors) and facilitated water splitting involving the oxidation of sacrificial chemical reagents. However, we are still collectively

looking for a practical solution without the use of platinum group metals for PC or PEC water splitting to produce a viable non-nuclear energy source for the long-term future (e.g., according to the Web of Science more than 3000 scientific papers have been published based on the use of three key words: solar, semiconductor, and H_2). These limited sub-set of papers have accumulated more than 142,000 total citations since 1976. Key challenges that must still be overcome include: 1) utilization of earth-abundant but low-cost semiconductor photocatalysts, 2) increase solar light capture efficiency over the wavelength range of 500 to 800 nm, 3) reduce direct and indirect electron-hole recombination, 4) enhance interfacial electron transfer efficiency, and 5) increase overall quantum efficiencies of H_2 and O_2 production .

Titanium dioxide (TiO_2), because of its catalytic activity, high stability, and low cost, is often used as a photocatalyst or in PEC cells. However, the band gap of TiO_2 is 3.2 eV, which limits light absorption to the ultraviolet and limits its overall photocatalytic efficiency in terms of the solar spectrum [9]. After more than 40 years of systematic investigation of the catalytic properties of TiO_2, a variety of experimental methods have been developed in order to synthesize an array of different morphologies of TiO_2 such as nanotubes, nanorods, nanoplates, and nanoflowers in order to increase photocatalytic and electrocatalytic activity [10-12]. However, the various synthetic modifications have not done much to extend visible light absorption of TiO_2 above 450 nm. Thus, additional modifications methods have utilized metal doping, nonmetal doping, multiple dopants in an attempt to push light absorption and catalytic activity higher into the visible portion of the spectrum [13-15]. Recently, there are considerable efforts are devoted to enhance device performance in PEC generation of H_2 by the incorporation of carbonaceous

materials, such as multiwall carbon nanotubes (MWCNTs), graphene oxide and so on. Navarro-Pardo et al. [16] prepared graphene oxide/cobalt-based nanohybrid, which possessed stable PEC performance for H_2 generation. Selopal et al. [17] combined MWCNTs with TiO_2 and incorporated with $CdSe/(CdSe_xS_{1-x})_5/(CdS)_2$ colloidal quantum dots (QDs) for solar energy conversion to H_2 technology. Tong et al. [18] synthesized ZnS-CISeS QDs-based TiO_2 photoanode with high stable, used for device in H_2 production.

Among the above researches, substance including TiO_2 and carbonaceous materials showed superior H_2 generation. The metal or nonmetal materials doping can extend light absorption into the visible light and near-infrared region of the spectrum, but trapping states and carrier recombination after doping often limit photocatalytic activity. One of the options is to utilize the surface plasmon resonance (SPR) effect of metal combined with TiO_2 to extend light absorption range, in which Au, Pt, Ag all has the plamonic effect for collective oscillation of surface electrons transferred to TiO_2 under visible light [19-21]. Combinations of wide and narrow band gap heterojunction semiconductor composites have been used to enhance charge transfer and to reduce the electron-hole recombination coupled with improved light absorption in visible region. Cadmium sulfide (CdS), an n-type semiconductor, with a band gap of 2.4 eV has been used in various forms and composites as a H_2 evolution catalyst. CdS can be combined with TiO_2 to form a heterojunction that has been often used as a photocatalyst for solar H_2 production [22]. Although combining CdS with TiO_2 has been shown to retard photocorrosion and to improve the overall lifetime of the composite catalyst. In addition, the composite catalysts have been shown to visible light photocatalytic activity and enhance PEC performance of TiO_2 nanotube electrodes

[23-25]. Although the ternary heterostructures composed of CdS, mental and TiO_2 semiconductor were investigated for PEC activity, the utilization of them as photoanode for H_2 production with pollutant as holes sacrificial agent remains poorly explored.

In this study, TiO_2 nanorods (TiO_2-NRs) are combined with Ag nanoparticles and CdS to form CdS/Ag/TiO_2-NRs photo-electrodes. The characteristics and electrochemical properties of composite photo-electrodes were analyzed and their PEC activity with respect to H_2 evolution with visible light irradiation was studied. The effects of nanorods length and role of nitrobenzene (NB) as a sacrificial reagent for H_2 production were also investigated.

2. Experimental Methods

2.1 Preparation of CdS/Ag/TiO_2-NRs

TiO_2-NRs were prepared by hydrothermal method [11]. Fluorine doped tin oxide (FTO) electrode substrates with dimensions of 2 cm×5 cm were cleaned first by ultrasonic irradiation in acetone, ethyl alcohol, and deionized water each for 15 min and then dried in the air. 50 mL of 50% HCl solution was mixed in 10 min, and then 0.6 ml tetrabutyl titanate was added with stirring for 5 min. The pretreated FTO was placed in an autoclave along with 25 mL of the prepared solution and calcined at 170 °C for 4 h to form the TiO_2-NRs.

CdS/TiO_2-NRs were prepared by deposition of CdS on the surface of TiO_2-NRs in suspension. The solution suspension was composed adding 1.0 M aqueous ammonia in to 40 mL of distilled water along with 1.0 mM cadmium sulfate, 5 mM sulfocarbamide, and TiO_2-NRs. This suspension was heated at 60 °C for 10 min. The filtered suspension of CdS on TiO_2-NRs was calcined at 400 °C in N_2 for 2 h to produce the final product CdS/TiO_2-NRs. Ag/TiO_2-NRs

was prepared by UV reduction of 40 g/L $AgNO_3$ in the presence of TiO_2-NRs. The mixed suspension was stirred in dark for 1 h and then illuminated for 0.5 h using a 500 W Xenon photolysis lamp in order to produce Ag nanoparticles loaded on to TiO_2-NRs.

The hybrid CdS/Ag/TiO_2-NR catalyst was prepared by deposition of CdS on to the surface of Ag/TiO_2-NRs in an aqueous suspension. After deposition of CdS, the mixture was calcined at 400 °C under N_2 for 2 h resulting in the formation of CdS/Ag/TiO_2-NRs. The experimental procedure is depicted in Scheme 1.

Scheme 1

2.2 Characterization of CdS/Ag/TiO_2-NRs electrode

The crystalline phase was determined by X-ray diffractometer (XRD), while the crystal lattice and fringe phases were determined by transmission electron microscope (TEM). The modified electrode surface was further characterized by X-ray photoelectron spectroscopy (XPS). The morphology structure of the modified electrode surface was characterized by field emission scanning electron microscope (SEM) and EDS map. The surface spectral properties of photocatalytic electrode material were analyzed by UV-Vis diffuse reflectance spectrometer (UV-Vis).

2.3 Photoelectrochemical Properties (PEC)

All of the PEC tests were carried out in a three-electrode configuration where the prepared electrode was working electrode, Pt was counter electrode, and Ag/AgCl was reference electrode. Under the illumination, Xenon lamp produced visible light at an intensity of 100 mW cm^{-2}. Photocurrent density (J-V) of the CdS/Ag/TiO_2-NR electrode was determined by linear

sweep voltammetry of a 0.1 M electrolyte containing Na_2S and Na_2SO_3 in solution (pH 13.03) in the absence of NB with a sweep range from -1.0 V to 0.6 V. The current density is reproducible and stable, within an acceptable range error of 5%. Electrochemical impedance spectroscopy (EIS), Mott-Schottky (M-S) curves, light conversion efficiencies, and monochromatic incident photon-to-electron conversion efficiencies (IPCE) were determined using the same electrolyte at a bias voltage of 0.4 V and EIS frequency of 10^{-2}-10^{6}. M-S curves were obtained by the impedance-potential technique at a voltage range of -1.0 V to 0.4 V and scan frequencies of 1000, 2000 and 3000 Hz under dark conditions.

2.4 H_2 Production and Oxidation of Nitrobenzene (NB)

The formation of H_2 and degradation of NB were tested to analyze the PEC activity of CdS/Ag/TiO_2-NRs. NB was selected as the electron donor (i.e., a sacrificial reagent) to promote the separation of electron-hole pairs, so that photo-induced electron could be transferred to the cathode to H_2.

The CdS/Ag/TiO_2-NR electrode was used as the anode with an effective geometric electrode surface area of 4 cm^2. And foam nickel was pure and no electrocatalyst was deposited on it, which was used as cathode with the electrode distance of 2 cm. All of the PEC tests were carried under visible light irradiation at λ> 420 nm and bias voltage of 0.5 V. The PEC tests were carried out using online detection of H_2 production under a slight vacuum. H_2 was analyzed by gas chromatography (GC) with N_2 as the carrier gas at a gas pressure of 0.1 MPa and detector temperature of 110 °C. The electrolyte solution consisted of 30 mg L^{-1} of NB in 0.5 M Na_2S and Na_2SO_3 solution (pH 13.64). The concentration of NB was analyzed by high performance liquid

chromatography (HPLC) with Diamonsil C18 reverse column and detection wavelength of 262 nm. The ratio of mobile phase of methanol: deionized water: glacial acetic acid is 49: 50: 1 with the flow rate of 1 mL min^{-1}.

3. Results and Discussion

3.1 Electrode Materials Characterization

3.1.1 Elements analyses

Figure S1 shows the XRD patterns of TiO_2-NRs, Ag/TiO_2-NRs, CdS/TiO_2-NRs and CdS/Ag/TiO_2-NRs electrodes. It can be seen that an adsorption peak at 2θ = 26.5º corresponding as CdS (002) [26,27] is present on CdS/TiO_2-NRs and CdS/Ag/TiO_2-NRs electrodes. Ag presents at 2θ = 44.7º as the crystal face (200) of Ag on Ag/TiO_2-NRs and CdS/Ag/TiO_2-NRs electrodes indicating that metallic Ag was stable on composite electrodes whether CdS was loaded or not. Since the (200) Ag was low, XPS analysis was carried out for intensive study.

The XPS spectra of CdS/Ag/TiO_2-NRs with Ag, Cd and S elements are shown in Figure 1. The CdS/Ag/TiO_2-NRs electrode contains Ti, O, Ag, Cd and S with the main peak of C at 284.8 eV corresponding to calibration peak of C-1s. The binding energy peaks of Ag is 373.88 eV and 367.87 eV correspond to Ag $3d_{3/2}$ and Ag $3d_{5/2}$, respectively. This is consistent with metallic silver on the surface [28,29]. The binding energy peaks of Cd and S at 412.29 eV, 405.53 eV, 163.04 eV and 161.82 eV correspond to Cd $3d_{3/2}$, Cd $3d_{5/2}$, and S 2p, respectively [30-33]. These results confirm that CdS and Ag are loaded on the surface of the TiO_2-NRs.

Figure 1

3.1.2 Microstructures

Figure 2 shows the SEM imagines of TiO_2-NRs, Ag/TiO_2-NRs, CdS/TiO_2-NRs, and CdS/Ag/TiO_2-NRs. As shown in longitudinal section imagines of the electrodes in Figure 2, TiO_2 deposited first on the base of FTO. After the growing the thickness of the TiO_2 film to greater than 450 nm, the TiO_2-NRs started to grow vertically and the length of TiO_2-NRs was about 1.2 μm with diameters close to 100 nm. Figure 2a and b depict the growth of TiO_2-NRs uniformly on FTO. Figure 2c and d show the Ag particles uniformly uploaded on the surface and interval of TiO_2-NRs. The pattern of CdS/TiO_2-NRs was similar with that of TiO_2-NRs as shown in Figure 2e and f. This indicates that CdS was synthesized as film covering the surface of the TiO_2-NRs. There is a co-loading of CdS and Ag on the surface of TiO_2-NRs (Figure 2g and h). In these cases, the Ag nanoparticles were observed and the CdS film covered both Ag and TiO_2-NRs. In addition, EDS mapping of section SEM image for CdS/Ag/TiO_2-NRs also confirmed the evenly distribution of Ag and CdS inside the TiO_2-NRs (Figure S2).

Figure 2

In addition, the effect of the reaction time for TiO_2-NRs growth was investigated as the growth length of TiO_2-NRs was higher with longer reaction times. Figure S3 shows the SEM images of CdS/Ag/TiO_2-NRs at different growth times of the TiO_2-NRs. All of CdS/Ag/TiO_2-NRs electrodes were loaded with Ag nanoparticles as shown both on top and on the vertical profile of the TiO_2-NRs. At a growth time for the TiO_2-NRs of 3 h, the nanorods were slender and skewed as shown in Figure S3 a and b. When the growth time of TiO_2-NRs was 4 h, the nanorods grew regularly with high surface area and Ag nanoparticles uniformly loaded on the surface of nanoroads shown in Figure S3 c and d. As shown in Figure S3 e-h, when the growth time of

196 TiO_2-NRs was longer than 4 h, the diameters and lengths of nanorods increased and the gaps
197 among the nanoroads decreased. In this case, the Ag nanoparticles were mainly loaded on the top
198 of the TiO_2-NRs and the intervening gaps were filled with CdS.

199 The further understand the composite structure and morphology, TEM images of
200 CdS/Ag/TiO_2-NRs were obtained and summarized in Figure 3a and b. These figures show the
201 overall morphology of CdS/Ag/TiO_2-NRs as a function of the magnifications level is consistent
202 with the loading of Ag CdS film on the surface the TiO_2-NRs. Figure 3c shows the partial
203 enlargement of TEM image of CdS/Ag/TiO_2-NRs in which a CdS film appears to cover the
204 TiO_2-NRs and also the Ag nanoparticles. Using DigitalMicrograph software, the spacing of the
205 lattice fringes are determined to be 0.325 nm, 0.237 nm, and 0.341 nm corresponding to TiO_2
206 (110) [34], Ag (200) [35], and CdS (002) [36] crystalline facets, respectively. These results are
207 consistent with XRD and XPS observations.

208 Figure 3

209 3.1.3 Optical Absorption

210 Figure 4 shows the UV-vis diffuse reflectance spectra of TiO_2-NRs, Ag/TiO_2-NRs,
211 CdS/TiO_2-NRs, and CdS/Ag/TiO_2-NRs over the wavelength range of 250 to 850 nm. The inset
212 plot provides the Kubelka−Munk transformed reflectance spectra for the different electrodes.
213 Bare TiO_2-NRs absorb light mainly in the ultraviolet region with a band gap energy of 3.02 eV.
214 The absorption spectrum of Ag/TiO_2-NRs was red shifted toward 500 nm with a corresponding
215 band gap energy of 2.32 eV, which may be due in part to the SPR effect of noble metal element
216 Ag combined with n-type semiconductor TiO_2 with the SPR peak at approximately 470 nm. In

addition, the band energy gap of CdS is 2.4 eV. The cumulative effect is a shifting of absorption spectrum $\lambda < 500$ nm [37, 38]. For the comparison, the band gap energy of CdS/TiO_2 was determined to be 2.25 eV. When Ag and CdS are combined with TiO_2-NRs, the adsorption spectrum of composite or hybrid material CdS/Ag/TiO_2-NRs shifted even further to 700 nm with an energy gap of 1.57 eV. The strong absorption peak near 600 nm is attributed to the SPR effects of the Ag nanoparticles. The red shifted of peak due to the CdS layer enveloping the Ag nanoparticles has a large refractive index. Thus, the addition Ag results in a hetero-junction catalyst when combined with CdS/TiO_2-NRs that is enhanced in due to the impact of SPR excitation and improved electron transfer rates due to the lowering of the Shottky barrier lowing effect of Ag to the base support.

Figure 4

Figure S4 shows the UV-vis diffuse reflectance spectrum of CdS/Ag/TiO_2-NRs versus time of composite growth over the wavelength range of 220 to 850 nm. The CdS/Ag/TiO_2-NR composite has its highest absorption over the range of 500-700 nm that takes place at a time less than 4 h of sintering. This effect is most likely due to several factors. At growth time less than 4 h, the diameter and length of the nanorods quite small as shown in Figure S3 a and b with a corresponding high surface area and loading capacity. However, if the growth time is greater than 4 h, a lateral overgrowth of the nanorods occurs with an increase in diameter and a decrease in the gap distance between the nanorods (also shown in Figure S3 e-h). As a consequence, the specific surface area is less and the loading capacity decreases. Thus, the optimal nanorod structures are found near 4 h of net reaction time to form uniform TiO_2-NRs.

3.2 PEC properties of the electrodes

3.2.1 Photocurrent responses

The LSV of the CdS/TiO_2-NRs and CdS/Ag/TiO_2-NRs electrodes under visible or UV-Vis irradiation are shown in Figure 5a. The photocurrent density of CdS/Ag/TiO_2-NRs was almost double that of the CdS/TiO_2-NRs under both visible and UV-Vis irradiation. The photocurrent densities of TiO_2-NRs and Ag/TiO_2-NRs were barely detected under visible light irradiation. The photocurrent density of the composite CdS/Ag/TiO_2-NRs electrodes under the visible light irradiation ~12 mA cm^{-2} at a bias voltage of +0.6 V vs SCE, which is approximately 85% of photocurrent density under UV-Vis light irradiation (nearly 14 mA cm^{-2} at bias voltage of 0.6 V vs SCE). This result clearly shows that the CdS/Ag/TiO_2-NRs electrode has a significant visible light response capacity that allows for the PEC production of H_2 under visible light irradiation. CdS, CdSe and their composites combined with TiO_2 (such as TiO_2/CdSe/$(CdSe_xS_{1-x})_5$/$(CdS)_2$ QD-MWCNT [17], CdS/CdSe/TiO_2 [39], CdSe/TiO_2 [40], PdS@CdS/ZnS/TiO_2 [41]) could yield higher than 10 mA cm^{-2} photocurrent density for H_2 formation by PEC process, so CdS/Ag/TiO_2-NRs prepared in our study (nearly 14 mA cm^{-2} at bias voltage of 0.6 V vs SCE) is similar with the references.

Li et al. [27] had prepared a CdS/Au/TiO_2-NT composite electrode with a high photocurrent response. We also prepared a CdS/Au/TiO_2-NTs electrode for comparison and measured the photocurrent as shown in Figure 5a. The photocurrent density of the CdS/Au/TiO_2-NTs electrode is lower than that of CdS/Ag/TiO_2-NRs but higher than that of CdS/TiO_2-NRs electrode. The Ag deposited between the TiO_2-NRs and overcoated CdS film results in more photo-generated

electrons produced by the SPR effect of Ag and the improved electron transfer rates between CdS and TiO_2-NRs.

Figure 5b shows LSV of CdS/Ag/TiO_2-NRs with different growth time at bias voltage of 0.4 V vs SCE. With the growth time increased to 4 h, the photocurrent density increased twice than that of 3 h and had little electron-hole recombination. Under a long time irradiation, the photocurrent density of CdS/Ag/TiO_2-NRs with growth time of 4 h maintained stable at about 9 mA cm^{-2}. At growth times greater than 4 h, the resulting photocurrent density of CdS/Ag/TiO_2-NRs electrodes decreased. It was probably due to the morphology change of CdS/Ag/TiO_2-NRs. At a growth time for the TiO_2-NRs of 3 h, the nanorods were short, thin and skewed, which limited the load of silver and CdS on the surface of TiO_2-NRs. When the growth time reached to 5 h, the crystal growth rate starts to decrease as the system approaches equilibrium resulting in TiO_2 film formation [11]. While, at the growth time of 4 h, TiO_2-NR were shape integrity with Ag and CdS distributed uniformly. In addition, the CdS/Ag/TiO_2-NR composite for 4 h sintering has the highest absorption over the range of 500-700 nm resulting in highest photocurrent density.

Figure 5

3.2.2 Electrochemical properties

Impedance and charge transfer characteristics of the composite electrodes where measured using EIS as shown in Figure S5. The results show that the ternary composite electrode has the smallest impedance radius compared to the binary electrodes, and the naked TiO_2-NRs electrode under both dark and light conditions. The low impedance of the CdS/Ag/TiO_2-NR electrode

bodes well for charge separation and subsequent electron and hole transfer with an applied bias potential [42-44].

The M-S curves obtained for the TiO_2-NRs (a), Ag/TiO_2-NRs (b), CdS/TiO_2-NRs (c) and CdS/Ag/TiO_2-NRs (d) electrodes are shown in Figure 6. The flat band potential, E_{fb}, of the bare TiO_2-NRs electrode is -0.34 V. Modification with Ag to form Ag/TiO_2-NRs shifts the E_{fb} to -0.74 V, which indicates that modified electrodes formed a Schottky barrier and that the Fermi level energies of Ag and TiO_2 were equal. Since the conduction band of CdS is more negative than TiO_2, the E_{fb} of CdS/TiO_2-NRs shifts negative to -0.59 V. Addition of Ag to CdS/TiO_2-NRs shifts the E_{fb} of CdS/Ag/TiO_2-NRs -0.78 V. The slightly more negative E_{fb} for CdS/Ag/TiO_2-NRs implies a stronger driving force for PEC H_2 generation.

Figure 6

3.2.3 Solar energy conversion efficiency

The photoconversion efficiency of the Ag/TiO_2-NRs, CdS/TiO_2-NRs and CdS/Ag/TiO_2-NRs electrodes was determined by the photocurrent as a function of the applied bias voltage [45-47], as shown in Eq. (1):

$$\eta(\%) = j_p[E^0_{rev} - |E_{app}|] \times 100/I_0 \quad (1)$$

where, j_p is the photocurrent density (mA cm^{-2}) under bias voltage, E^0_{rev} is the standard reversible potential (1.23 V vs. NHE), E_{app} is the applied potential (vs. SCE) calculated by the electrode work potential E_{meas} (vs. SCE) subtracting open circuit voltage E_{aoc} (vs. SCE), and I_0 is the instantaneous incident light intensity (100 mA cm^{-2}). As shown in Figure 7a and b, the photocoversion efficiency of the Ag/TiO_2-NR electrode virtually no photocurrent response under

visible light irradiation. At the bias voltage of 0.4 V vs. SCE, the photoconversion efficiency of the CdS/TiO_2-NR electrode reached a maximum of 2% while the CdS/Ag/TiO_2-NR electrode achieved a maximum efficiency of 4.4%. The CdS/Au/TiO_2-NT electrode as prepared by Li et al. [27] had a maximum photoconversion efficiency of 2.8%, while the photoconversion efficiency of our CdS/Ag/TiO_2-NR electrode was 1.5 times higher than the Au based electrode. This result shows that the intervening Ag nanoparticles between CdS and TiO_2-NRs improved the relative photoconversion efficiency.

Figure 7c shows the IPCE of TiO_2-NRs, Ag/TiO_2-NRs, CdS/TiO_2-NRs and CdS/Ag/TiO_2-NRs based electrodes. Naked TiO_2-NRs electrodes had very little absorption above 450 nm, but the IPCE of modified TiO_2-NRs electrodes were enhanced at 420-650 nm. In this case, CdS/Ag/TiO_2-NRs has a maximum IPCE = 43% at 470 nm. Figure 7d shows the IPCE enhancement factor of the various electrode formulations. The CdS/Ag/TiO_2-NRs electrode had the maximum enhancement factor of 112 times compared to the naked TiO_2-NRs electrode. For comparison, and the CdS/TiO_2-NRs electrode had a 90 times higher IPCE compared to the naked TiO_2-NRs electrode at $\lambda < 500$ nm. These results shown Ag nanoparticles not only extend the visible light response of the base TiO_2-NRs, but also enhance the IPCE of CdS/Ag/TiO_2-NRs composite electrode.

Figure 7

3.3 Production of H_2

In Figure 8a the PEC production of H_2 on the different electrode formulations is compared. The production H_2 on CdS/TiO_2-NRs is higher than that on Ag/TiO_2-NRs. The observed surface

area normalized rate of H_2 production was 0.05 mmol h^{-1} cm^{-2} in 1 h. However, as the photolytic reaction time increased, the production rate of H_2 decreased. This may be due to photo-corrosion. The addition of Ag nanoparticles to CdS/TiO_2-NRs resulted in a H_2 production rate that was slower than on CdS/TiO_2-NRs over the first 2 h, but at longer irradiation times the three component hybrid electrode obtained a d[H_2]/dt = 0.09 mmol h^{-1} cm^{-2}.

As shown in Figure 8b, the production of H_2 increased to maximum level on the CdS/Ag/TiO_2-NR electrode as the nano-rod growth time increased to 4 h. Beyond 4 h the production rate of H_2 decreased with further increases in growth time. The SEM images of the CdS/Ag/TiO_2-NRs as shown in Figure S1 grow uniformly up to 4 h and also have a relatively high specific surface area leading to a higher deposited level of Ag nanoparticles and a greater degree of coverage of the TiO_2-NRs by the deposited CdS films that in turn leads to an enhanced PEC production of H_2.

The production of H_2 on the CdS/Ag/TiO_2-NR electrode under EC, PC and PEC excitation is shown in Figure 8c. H_2 production is very low under PC and EC activation. However, under the PEC activation, H_2 production is substantial and a function of the external applied potential.

In Figure 8d the degradation of NB is 96% after 50 min of photo-electrochemical activation. In comparison, activation by photons or an applied potential alone achieves a degradation percentatge for NB of approximately 20% and 10%, respectively, after 50 min of excitation. In the absence of catalytic surface, NB was degraded 6% in 50 min in the electrolyte solution alone. The sacrificial reagents, HS^- and HSO_3^-/SO_3^{2-} are frequently used reducing agents. For example, nitrobenzene ($ArNO_2$) has a reported 6-electron reduction potential of +0.83 V, while H_2S going

to elemental sulfur has an oxidation potential of -0.14 V. Thus, the reduction of $ArNO_2$ with H_2S should result in $ArNH_2$ (i.e., aniline) as follows: $ArNO_2 + 3H_2S \rightleftharpoons ArNH_2 + 3S^o + 2H_2O$. ($E^o_r$ = +0.69 V). Alternative reduction products of $ArNO_2$ reacting with H_2S would be ArNO (nitrosobenzene) and ArNHOH (phenyl hydroxl amine) on the way to $ArNH_2$ [48,49].

Figure 8

The impact of NB addition on the observed H_2 production rate is shown in Figure S6. However, the addition of NB did not appreciably affect H_2 production rate, although the amount of H_2 produced with additional NB was more than in the absence of NB. The photocurrent density obtained in the presence or in the absence of NB was shown in Figure S7 also shows that the presence of NB has no significant effect on the current density, only a small higher than the absence of NB, which was similar with the effect of H_2 production. In addition, NB appears to impede the photo-corrosion of CdS.

The stability of the CdS/Ag/TiO_2-NR electrode in terms of H_2 production over six cycles carried out in mixture of 0.5 M Na_2S and Na_2SO_3 in the presence of 30 mg L^{-1} of NB was determined. As shown in Figure S8, the composite CdS/Ag/TiO_2-NR electrode is stable for more than 30 h of total reaction. The Faradaic efficiency η of H_2 was calculated and depicted in Fig. S9 reached 65.83% after 6 h and the picture of production of H_2 on the foam nickel was shown in Fig. S10. Since the current is displayed directly at the power supply with two-electrode system but not a three electrode cell configuration, the Faradaic efficiency is calculated slightly low.

3.4 Proposed PEC mechanism of CdS/Ag/TiO_2-NRs for H_2 production

363 CdS is a narrow gap semiconductor, which is susceptible to photo-corrosion especially under
364 high light intensities. This problem can be overcome by using sacrificial electron donors such as
365 Na_2S and Na_2SO_3 for trapping the valence-band hole and preventing the oxidation of sulfide to
366 sulfate within the solid phase. In our study, nitrobenzene serves as an electron donor (i.e., a
367 sacrificial reagent) instead of S^{2-}/SO_3^{2-} that reacts with a surface trapped hole and transfers an
368 electron to the high redox potential hole. On the one hand, electron-hole pairs were separated and
369 photo-induced electron was transferred to the cathode for H_2 production. At the same time, NB is
370 oxidized further due to a diffusion controlled reaction with oxygen.

371 A plausible mechanism for the electro-catalytic reactions taking place on photo-activated
372 CdS/Ag/TiO_2-NRs is shown in Scheme 2. Under the visible light irradiation condition, CdS
373 absorbs over a broad range to produce conduction band electrons within CdS that can be further
374 captured by Ag. In addition, the SPR phenomenon formed by a combination of Ag and an n-type
375 semiconductor (e.g., TiO_2) generates additional electrons for water or proton reduction.

376 Scheme 2

377 Photo-activation of CdS/Ag/TiO_2-NRs results in little H_2 production. However, under an
378 applied potential bias, photo-generated electrons in the conduction band of CdS are transferred to
379 first to Ag and then subsequently to TiO_2, and then to the cathode resulting in the generations of
380 H_2. An additional driving force is provided by the impact of SPR taking place on Ag, which
381 leads to facilitated transfer to TiO_2, which is attached to the cathode surface. Surface bound $Ag^{+\cdot}$
382 formed because of the SPR effect can be reduced back to Ag^0 as mediated by CdS.

383 The most likely sequence of reaction steps are as follows:

$$CdS + hv \rightarrow CdS\ (h^+) + CdS\ (e^-) \quad (2)$$

$$CdS\ (e^-) + Ag \rightarrow Ag\ (e^-) + CdS \quad (3)$$

$$Ag\ (e^-) + TiO_2 \rightarrow TiO_2\ (e^-) + Ag \quad (4)$$

$$Ag + hv \rightarrow Ag^* \quad (5)$$

$$Ag^* + TiO_2 \rightarrow Ag^{+\cdot} + TiO_2\ (e^-) \quad (6)$$

$$Ag^{+\cdot} + CdS \rightarrow Ag + CdS\ (h^+) \quad (7)$$

$$TiO_2\ (e^-) \rightarrow \text{external circuit} \rightarrow \text{cathode}\ (e^-) \quad (8)$$

$$e^- + H^+ \rightarrow \tfrac{1}{2}H_2\uparrow \quad (9)$$

$$h^+ + NB \rightarrow \ldots\ldots \rightarrow \text{small molecular byproducts} \rightarrow \ldots\ldots \rightarrow CO_2 + H_2O \quad (10)$$

4. Summary

A composite electrode composed of CdS/Ag/TiO_2-NRs was synthesized and characterized. Based on TiO_2-NRs at a growth time of 4 h, ternary composite electrode showed the best PEC performance. The production of H_2 reached 2.24 mmol under 6 h visible light irradiation with the production rate of 0.09 mmol h^{-1} cm^{-2}. Its PEC activity was quantified and shown to be effective for H_2 production combined with the degradation of nitrobenzene. The enhanced electrochemical activity is attributed to: 1) the formation of Schottky bridge between silver and the n-type semiconductor, titanium dioxide, which resulted in a SPR effect that extended the visible light absorption range up to 700 nm for the semiconductor electrode; and 2) the improved charge-transfer rate due to the low Schottky barrier of the Ag-composite that effectively inhibited the electron-hole recombination. Since the CdS/Ag/TiO_2-NRs electrode could produce H_2 accompanied by degradation of NB under visible light irradiation, it would be probably using

other contaminants as sacrificial reagent rather than sodium sulfide and sodium sulfite for H_2 production in the future. It is a prospective material for solar H_2 production combined with pollutants degradation in order to greatly reduce the energy consumption and eliminate environmental pollutants.

Acknowledgements

The authors would like to acknowledge financial support for this work provided by Zhejiang Provincial Natural Science Foundation of China (Grant No. LY16B060001 and Y18B060003), National Nature Science Foundation of China (No. 21876154) and China Scholarship Council (No. 201708330449).

Supplementary Information (SI)

Supplementary material related to this article can be found online.

References:

[1] A. Gomez Vidales, S. Omanovic, Evaluation of nickel-molybdenum-oxides as cathodes for hydrogen evolution by water electrolysis in acidic, alkaline, and neutral media, Electrochim. Acta 262 (2018) 115-123.

[2] H. Inoue, T. Yamazaki, T. Kitamura, M. Shimada, M. Chiku, M., E. Higuchi, Electrochemical hydrogen production system from ammonia borane in methanol solution, Electrochim. Acta 82 (2012) 392-396.

[3] A.M. El-Melih, A. Al Shoaibi, A.K. Gupta, Hydrogen sulfide reformation in the presence of methane, Appl. Energy 178 (2016) 609-615.

[4] S. Xiu, J. Yao, G. Wu, Y. Huang, B. Yang, Y. Huang, L. Lei, Z. Li, Y. Hou,

426 Hydrogen-mediated electron transfer in hybrid microbialinorganic system and application in
427 energy and environment, Energy Technol. 7 (2019) 1800987-1800995.
428 [5] X. Liang, J. Liu, D. Zeng, C. Li, S. Chen, H. Li, Hydrogen generation promoted by
429 photocatalytic oxidation of ascorbate and glucose at a cadmium sulfide electrode. Electrochim.
430 Acta 198 (2016) 40-48.
431 [6] C.Y. Yang, Z. Wang, T.Q. Lin, H. Yin, J, Core-Shell nanostructured "Black" rutile titania as
432 excellent catalyst for hydrogen production enhanced by sulfur doping, Am. Chem. Soc.
433 135 (2013) 17831-17838.
434 [7] E. Baur, A. Rebmann, Über Versuche zur Photolyse des Wasser, Helv. Chim. Acta 4 (1921)
435 256-262.
436 [8] A. Fujishima, K. Honda, Electrochemical evidence of the mechanism of the primary stage of
437 photosynthesis, Bull. Chem. Soc. Japan 44 (1971) 1148-1150.
438 [9] J.H. Park, S.W. Kim, A.J. Bard, Novel carbon-doped TiO_2 nanotube arrays with high aspect
439 ratios for efficient solar water splitting, Nano. Lett. 6 (2006) 24-28.
440 [10] Z.R.R. Tian, J.A. Voigt, J. Liu, B. Mckenzie, Large oriented arrays and continuous films of
441 TiO_2-based nanotubes, J. Am. Chem. Soc. 125 (2003) 12384-12385.
442 [11] B. Liu, E.S. Aydil, Growth of oriented single-crystalline rutile TiO_2 nanorods on transparent
443 conducting substrates for dye-sensitized solar cells, J. Am. Chem. Soc. 131 (2009) 3985-3990.
444 [12] D. Reyes-Coronado, G. Rodríguez-Gattorno, M.E. Espinosa-Pesqueira, Phase-pure TiO_2
445 nanoparticles: anatase, brookite and rutile, Nanotechnology 19 (2008) 145605-145615.
446 [13] M. Murdoch, G.I.N. Waterhouse, M.A. Nadeem1, J.B. Metson, The effect of gold loading

447 and particle size on photocatalytic hydrogen production from ethanol over Au/TiO_2 nanoparticles,
448 Nat. Chem. 3 (2011) 489-492.
449 [14] C.Z. Wen, Q.H. Hu, Y.N. Guo, X.Q. Gong, From titanium oxydiflfluoride ($TiOF_2$) to titania
450 (TiO_2): phase transition and non-metal doping with enhanced photocatalytic hydrogen (H_2)
451 evolution properties, Chem. Commun. 47 (2011) 6138-6140.
452 [15] J. Hensel, G.M. Wang, Y. Li, J.Z. Zhang, Synergistic effect of CdSe quantum dot
453 sensitization and nitrogen doping of TiO_2 nanostructures for photoelectrochemical solar
454 hydrogen generation, Nano. Lett. 10 (2010) 478-483.
455 [16] G.S. Selopal, S.G. Cloutier, S. Sun, A.C. Tavares, H. Zhao, Z.M. Wang, F. Rosei, Graphene
456 Oxide/Cobalt-based Nanohybrid Electrodes for Robust Hydrogen Generation, Appl. Cata. B:
457 Environ. 245 (2019) 167-176.
458 [17] G.S. Selopal, M. Mohammadnezhad, F. Navarro-Pardo, F. Vidal, H. zhao, Z.M. Wang, F.
459 Rosei, Colloidal Heterostructured Quantum Dots Sensitized Carbon Nanotubes-TiO2 Hybrid
460 Photoanode for High Efficiency Hydrogen Generation, Nanoscale Horiz. 4 (2019) 404-414.
461 [18] X. Tong, Y. Zhou, L. Jin, K. Basu, R. Adhikari, G.S. Selopal, X. Tong, H. Zhao, S. Sun, A.
462 Vomiero, Z.M. Wang, F. Rosei, Heavy metal-free, near-infrared colloidal quantum dots for
463 efficient photoelectrochemical hydrogen generation. Nano Energy, 31 (2017) 441-449.
464 [19] Z.K. Zheng, B.B. Huang, X.Y. Qin, Facile in situ synthesis of visible-light plasmonic
465 photocatalysts M@TiO_2 (M ¼ Au, Pt, Ag) and evaluation of their photocatalytic oxidation of
466 benzene to phenol, J. Mater. Chem. 21 (2011) 9079-9087.
467 [20] Y. Wang, J. Zhai, Y.L. Song, Plasmonic cooperation effect of metal nanomaterials at

468 Au-TiO_2-Ag interface to enhance photovoltaic performance for dye sensitized solar cells, RSC
469 Adv. 5 (2015) 210-214.
470 [21] H.L. Ran, J.J. Fan, X.L. Zhang, Enhanced performances of dye-sensitized solar cells based
471 on Au-TiO_2 and Ag-TiO_2 plasmonic hybrid nanocomposites, Appl. Surf. Sci. 430 (2018)
472 415-423.
473 [22] D.R. Baker, P.V. Kamat, Adv. Photosensitization of TiO_2 nanostructures with CdS quantum
474 dots: Particulate versus tubular suppor architectures, Funct. Mater. 19 (2009) 805-811.
475 [23] H. Wang, Y.S. Bai, H. Zhang, Z.H. Zhang, CdS quantum dots-sensitized TiO_2 nanorod
476 array on transparent conductive glass photoelectrodes, J. Phys. Chem. C 114 (2010)
477 16451-16455.
478 [24] Y.K. Lai, Z.Q. Lina, D.J. Zheng, L.F. Chi, CdSe/CdS quantum dots co-sensitized TiO_2
479 nanotube array photoelectrode for highly effificient solar cells, Electrochim. Acta 79 (2012)
480 175-181.
481 [25] Y.X. Hu, B.Y. Wang, J.Q. Zhang, T. Wang, Synthesis and photoelectrochemical response
482 of CdS quantum dot-sensitized TiO_2 nanorod array Photoelectrodes, Nanoscale. Res. Lett. 8
483 (2013) 1-5.
484 [26] F.Q. Zhou, J.C. Fan, Q.J. Xu, Y.L .Min, $BiVO_4$ nanowires decorated with CdS
485 nanoparticles as Z-scheme photocatalyst with enhanced H_2 generation, Appl. Cata. B: Environ.
486 201 (2017) 77-83.
487 [27] J.T. Li, S.K. Cushing, P. Zheng, T. Senty, Solar hydrogen generation by a CdS-Au-TiO_2
488 sandwich nanorod array enhanced with Au nanoparticle as electron relay and plasmonic

489 photosensitizer. J. Am. Chem. Soc.136 (2014) 8438-8449.

490 [28] P.F. Tan, X. Chen, L.D. Wu, Y.Y. Shang, Hierarchical flower-like $SnSe_2$ supported Ag_3PO_4

491 nanoparticles:Towards visible light driven photocatalyst with enhanced performance, Appl. Cata.

492 B: Environ. 202 (2017) 326-334

493 [29] N.D. Feng, Q. Wang, A. Zheng, Z.F. Zhang, Understanding the High Photocatalytic

494 Activity of (B, Ag)-Codoped TiO_2 under Solar-Light Irradiation with XPS, Solid-State NMR,

495 and DFT Calculations, J. Am. Chem. Soc. 135 (2013) 1607-1616.

496 [30] L. Ge, F. Zuo, J.K. Liu, Q. Ma, C. Wang, Synthesis and Efficient Visible Light

497 Photocatalytic Hydrogen Evolution of Polymeric g-C_3N_4 Coupled with CdS Quantum Dots, J.

498 Phys. Chem. C 116 (2012) 13708-13714.

499 [31] L. Wu, J.C. Yu, X.Z. Fu, Characterization and photocatalytic mechanism of nanosized CdS

500 coupled TiO_2 nanocrystals under visible light irradiation, J. Mol. Catal. A-Chem. 244 (2006)

501 25-32.

502 [32] M.Z. Rong, M.Q. Zhang, H.C. Liang, H.M. Zeng, Surface modifification and particles size

503 distribution control in nano-CdS/polystyrene composite fifilm, Chem. Phys. 286 (2003) 267-276.

504 [33] C. Guillén, M. A. Martínez, C. Maffiotte, J. Herrero, Chemistry of CdS/$CuInSe_2$ Structures

505 as Controlled by the CdS Deposition Bath, J. Electrochem. Soc. 148 (2001) G602-G606.

506 [34] J.G. Yu, J.F. Xiong, B. Cheng, S.W. Liu, Fabrication and characterization of Ag-TiO_2

507 multiphase nanocomposite thin films with enhanced photocatalytic activity, Appl. Cata. B:

508 Environ. 60 (2005) 211-221.

509 [35] K. Li, T.Y. Peng, Z.H. Ying, S.S. Song, J. Zhang, Ag-loading on brookite TiO_2 quasi

510 nanocubes with exposed {210} and {001} facets: Activity and selectivity of CO_2 photoreduction
511 to CO/CH_4, Appl. Cata. B: Environ. 180 (2016) 130-138.
512 [36] M.M. Guo, L.Y. Wang, Y. Xia, W. Huang, Z.L. Li, Enhanced photoelectrochemical
513 properties of nano-CdS sensitized micro-nanoporous TiO_2 thin films from gas/liquid interface
514 assembly, J. Alloy. Compd. 684 (2016) 616-623.
515 [37] H. Tada, T. Mitsui, T. Kiyonaga, All-solid-state Z-scheme in CdS-Au-TiO_2
516 three-component nanojunction system, Nat. Mater. 5 (2006) 782-786.
517 [38] H.W. Park, W.Y. Choi, M.R. Hoffmann, Effects of the preparation method of the ternary
518 CdS/TiO_2/Pt hybrid photocatalysts on visible light-induced hydrogen production, J. Mater.
519 Chem. C 18 (2008) 2379-2385.
520 [39] Y.L. Lee, C.F. Chi and S.Y. Liau, CdS/CdSe Co-Sensitized TiO_2 Photoelectrode for
521 Efficient Hydrogen Generation in a Photoelectrochemical Cell, Chem. Mater. 22 (2010)
522 922-927.
523 [40] H.-J. Ahn, M.-J. Kim, K. Kim, M.-J. Kwak, J.-H. Jang, Optimization of Quantum
524 Dot-Sensitized Photoelectrode for Realization of Visible Light Hydrogen Generation, Small 10
525 (2014) 2325-2330.
526 [41] L. Jin, B. AlOtaibi, D. Benetti, S. Li, H. Zhao, Z. Mi, A. Vomiero, F. Rosei, Near-Infrared
527 Colloidal Quantum Dots for Efficient and Durable Photoelectrochemical Solar-Driven Hydrogen
528 Production, Adv. Sci. 3 (2016) 1500345-1500352.
529 [42] X. Yu, R. Du, B. Li B, Biomolecule-assisted Self-assembly of CdS/MoS_2/Graphene Hollow
530 Spheres as High-Efficiency Photocatalysts for Hydrogen Evolution without Noble Metals, Appl.

Cata. B: Environ. 182 (2016) 504-512.

[43] B.L. He, B. Dong, H.L. Li, Preparation and electrochemical properties of Ag-modified TiO_2 nanotube anode material for lithium-ion battery, Electrochem. Comm. 9 (2007) 425-430.

[44] Y.H. Jang, X.K. Xin, M. Byun, Y.J. Jang, Z.Q. Lin, An Unconventional Route to High-Efficiency Dye-Sensitized Solar Cells via Embedding Graphitic Thin Films into TiO_2 Nanoparticle Photoanode, Nano. Lett. 12 (2012) 479-485.

[45] B. Huang, W.J. Yang, Y.W. Wen, B. Shan, Co_3O_4-Modified TiO_2 Nanotube Arrays via Atomic Layer Deposition for Improved Visible-Light Photoelectrochemical Performance, ACS Appl. Mater. Interfaces 7 (2015) 422-431.

[46] D. Esparza, I. Zarazúa, T. Lopez-Luke, A. Cerdán, Effect of Different Sensitization Technique on the Photoconversion Efficiency of CdS Quantum Dot and Cdse Quantum Rod Sensitized TiO_2 Solar Cells, J. Phys. Chem. C 119 (2005) 13394-13403.

[47] G.M. Wang, H.Y. Wang, Y.C. Ling, Y.C. Tang, Hydrogen-Treated TiO_2 Nanowire Arrays for Photoelectrochemical Water Splitting. Nano Lett. 11 (2011) 3026-3033.

[48] A. Agrawal, P.G. Tratnyek, Reduction of nitro aromatic compounds by zero-valent iron metal, Environ. Sci. Technol. 30 (1996) 153-160.

[49] F.M. Dunnivant, R.P. Schwarzenbach, D.L.Macalady, Reduction of substituted nitrobenzenes in aqueous solutions containing natural organic-matter, Environ. Sci. Technol. 26 (1992) 2133-2141.

Figure captions:

Scheme 1 The experimental preparation diagram of CdS/Ag/TiO_2-NRs

Figure 1 XPS of overview element (a), Ag (b), Cd (c), S (d) of the CdS/Ag/TiO_2-NTs electrode

Figure 2 Front (left) and section (right) SEM of TiO_2-NRs (a, b), Ag/TiO_2-NRs (c, d), CdS/TiO_2-NRs (e, f) CdS/Ag/TiO_2-NRs (g, h)

Figure 3 TEM of CdS/Ag/TiO_2-NRs electrode (a, b), the partial enlargement of CdS/Ag/TiO_2-NRs (c) and HRTEM image of CdS/Ag/TiO_2-NRs (d)

Figure 4 UV-visible diffuse reflectance spectrum and the corresponding Kubelka−Munk transformed reflectance spectra (inset picture) of TiO_2-NRs, Ag/TiO_2-NRs, CdS/TiO_2-NRs and CdS/Ag/TiO_2-NRs

Figure 5 LSV of different electrodes under visible light or UV-Vis irradiation (a) and CdS/Ag/TiO_2-NRs with different growth time under visible light irradiation (b) (electrolyte: 0.1 M Na_2S and Na_2SO_3, pH 13.03, light density: 100 mW cm^{-2})

Figure 6 Mott-Schottky curve of TiO_2-NRs (a), Ag/TiO_2-NRs (b), CdS/TiO_2-NRs (c) and CdS/Ag/TiO_2-NRs (d) (electrolyte: 0.1 M Na_2S and Na_2SO_3)

Figure 7 Current density (a), photoconversion efficiency (b), IPCE (c) and IPCE enhancement factor (d) of different electrodes (electrolyte: 0.1 M Na_2S and Na_2SO_3, pH 13.03, light density: 100 mW cm^{-2})

Figure 8 H_2 generation by Ag/TiO_2-NRs, CdS/TiO_2-NRs and CdS/Ag/TiO_2-NRs electrodes (a), by CdS/Ag/TiO_2-NRs with different growth time, production of H_2 (c) and degradation of NB (d) with CdS/Ag/TiO_2-NRs under EC, PC and PEC processes (electrolyte: 0.5 M Na_2S and Na_2SO_3 and 30 mg L^{-1} NB, pH 13.64, light power: 500 W high pressure Hg lamp > 420 nm)

Scheme 2 Possible hydrogen production mechanism diagram

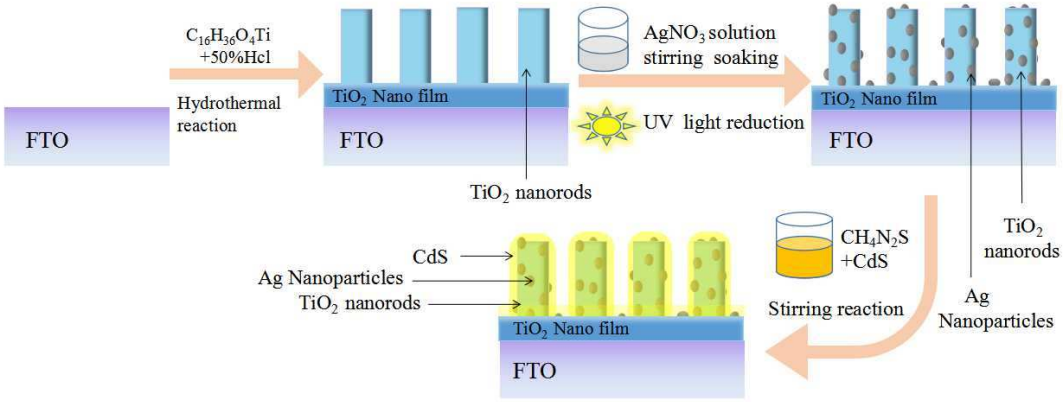

Scheme 1

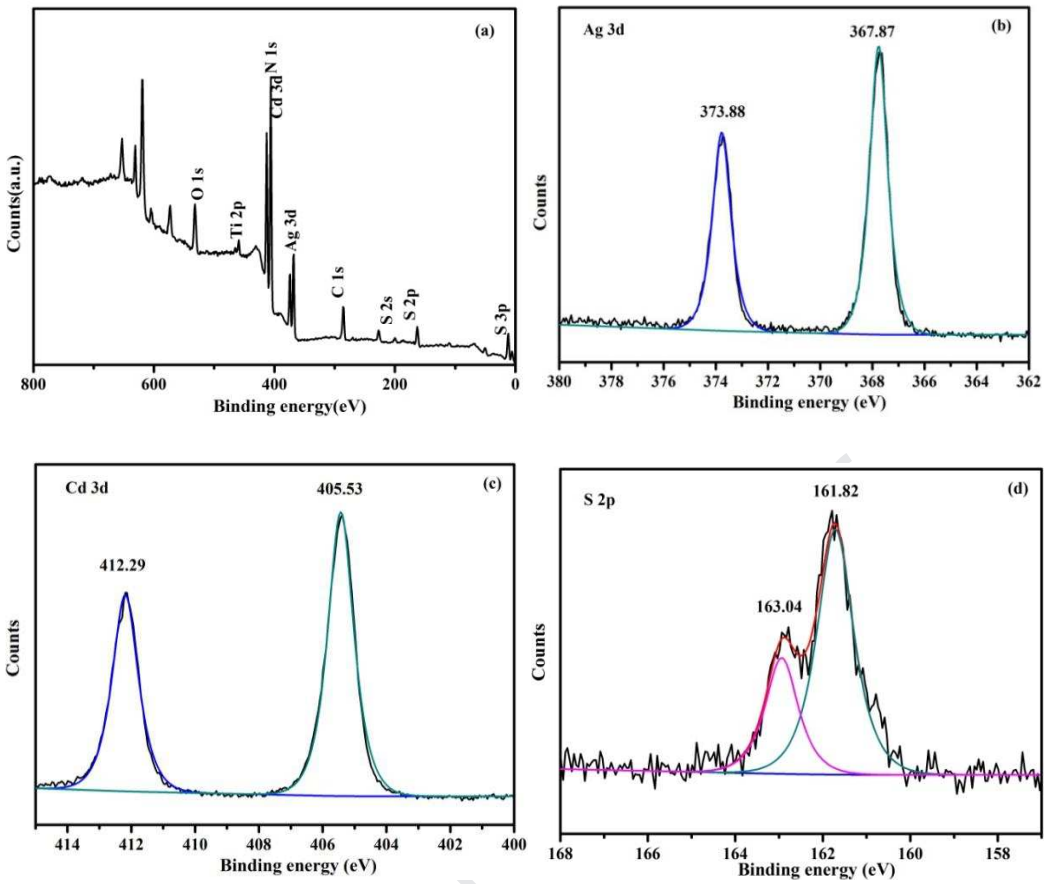

Figure 1

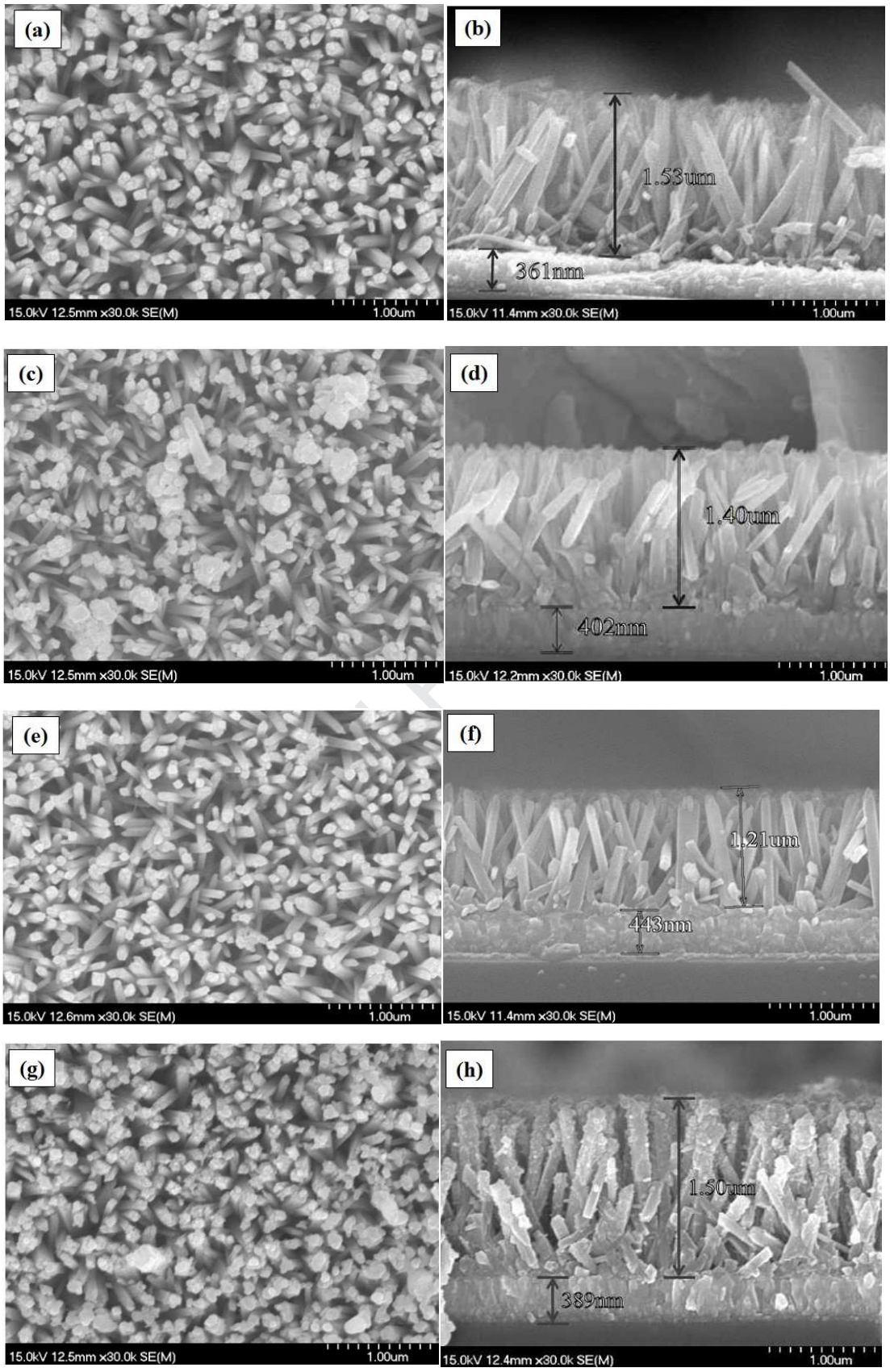
(a)
15.0kV 12.5mm x30.0k SE(M)
1.00um
(b)
1.53um
361nm
15.0kV 11.4mm x30.0k SE(M)
1.00um
(c)
15.0kV 12.5mm x30.0k SE(M)
1.00um
(d)
1.40um
402nm
15.0kV 12.2mm x30.0k SE(M)
1.00um
(e)
15.0kV 12.6mm x30.0k SE(M)
1.00um
(f)
1.21um
443nm
15.0kV 11.4mm x30.0k SE(M)
1.00um
(g)
15.0kV 12.5mm x30.0k SE(M)
1.00um
(h)
1.50um
389nm
15.0kV 12.4mm x30.0k SE(M)
1.00um

Figure 2

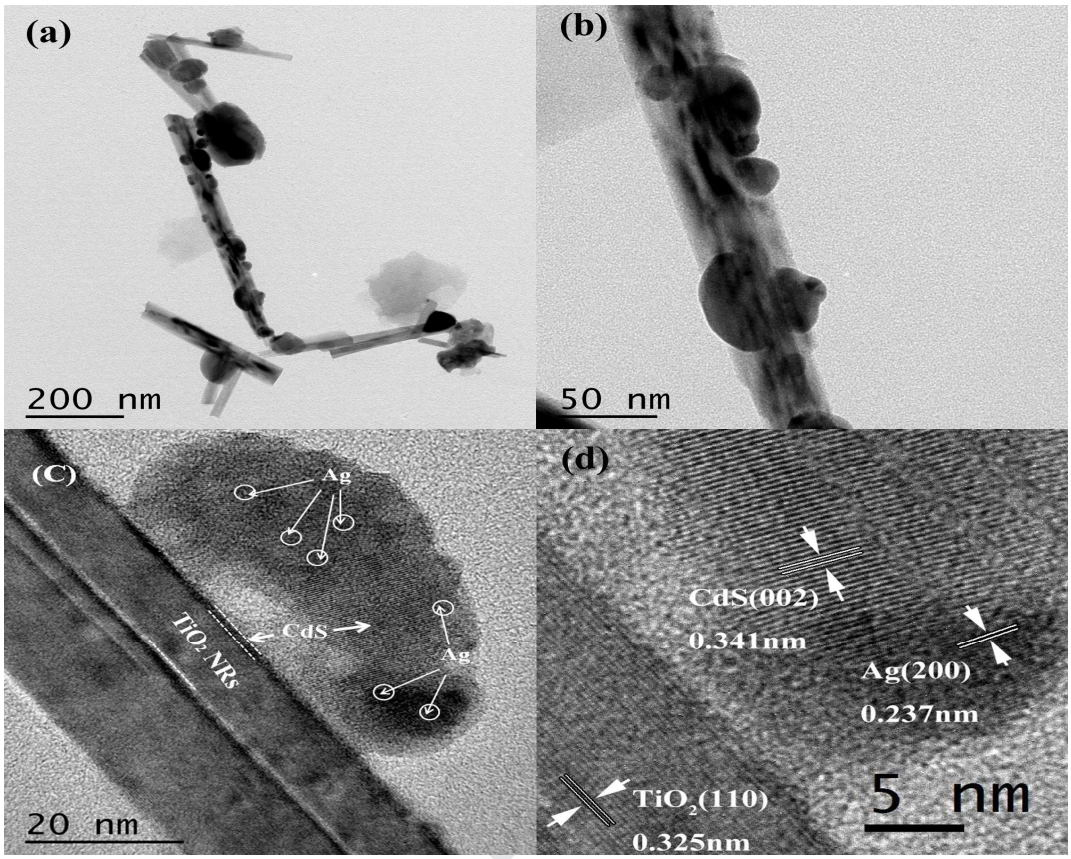

Figure 3

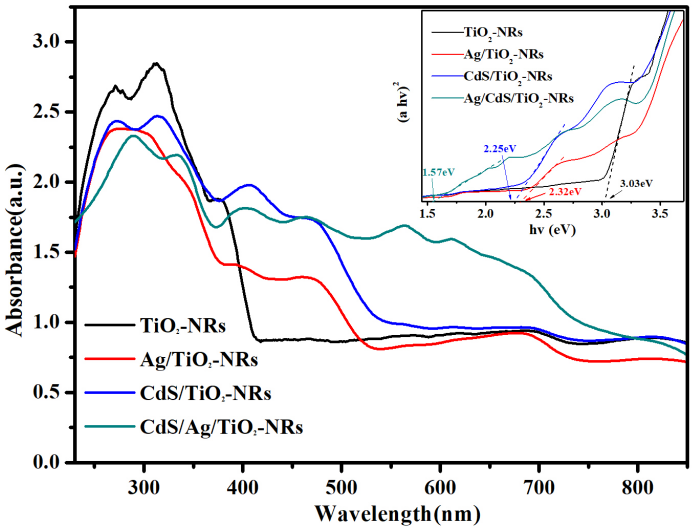

Figure 4

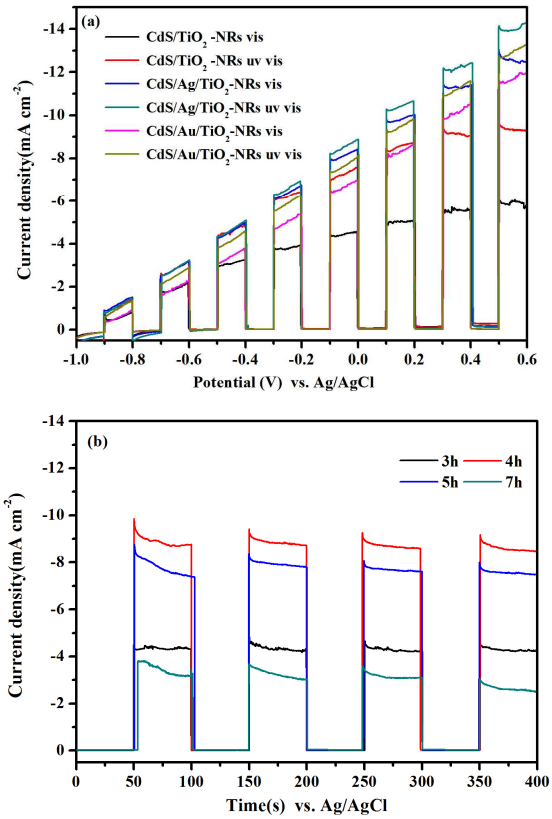

Figure 5

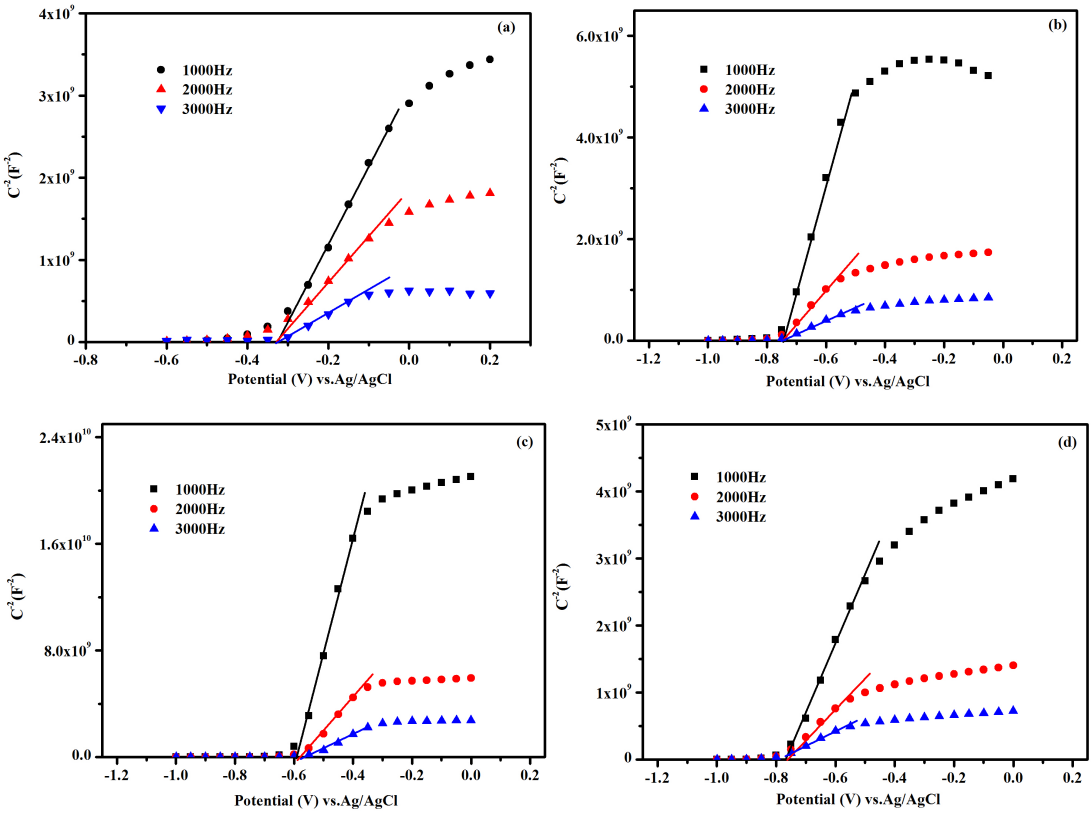

Figure 6

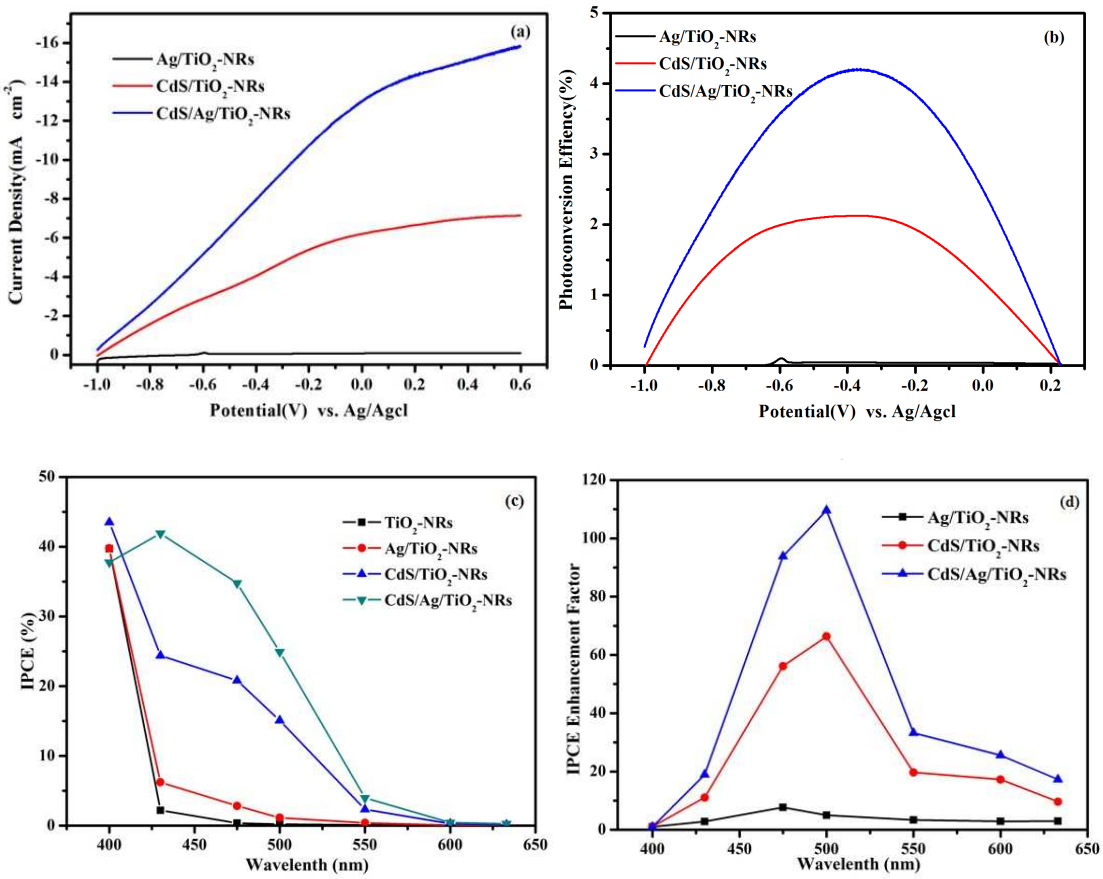

Figure 7

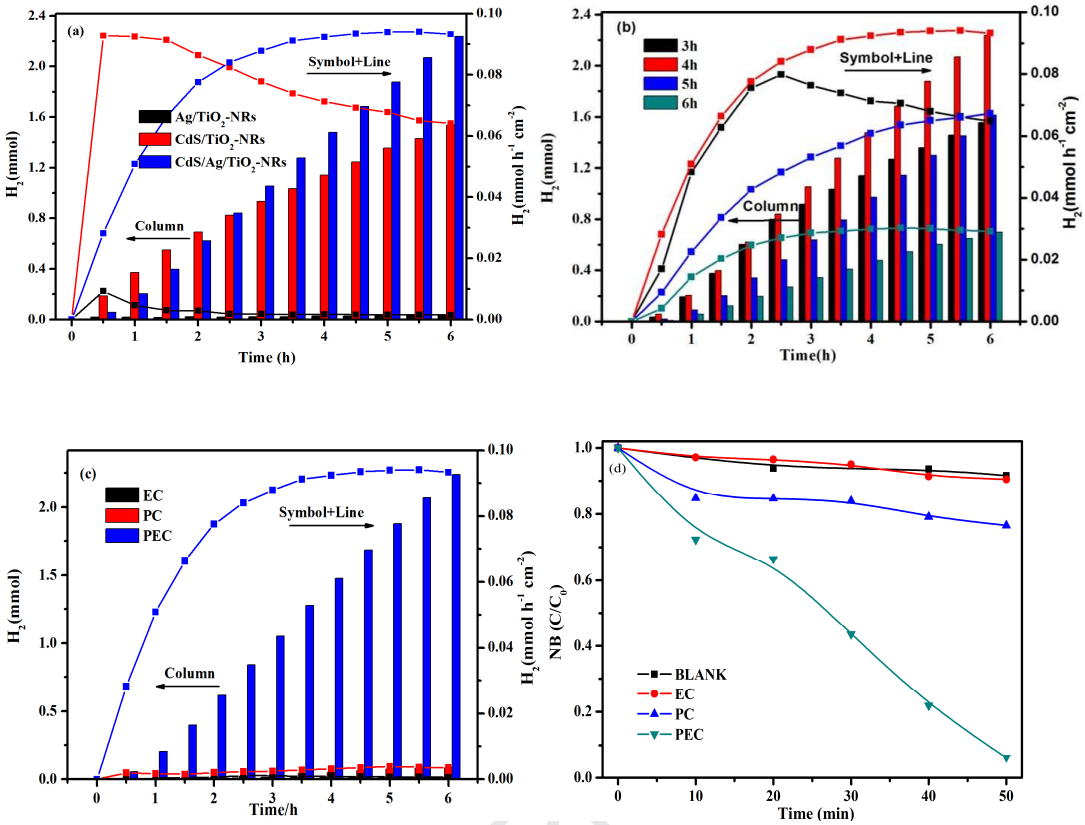

Figure 8

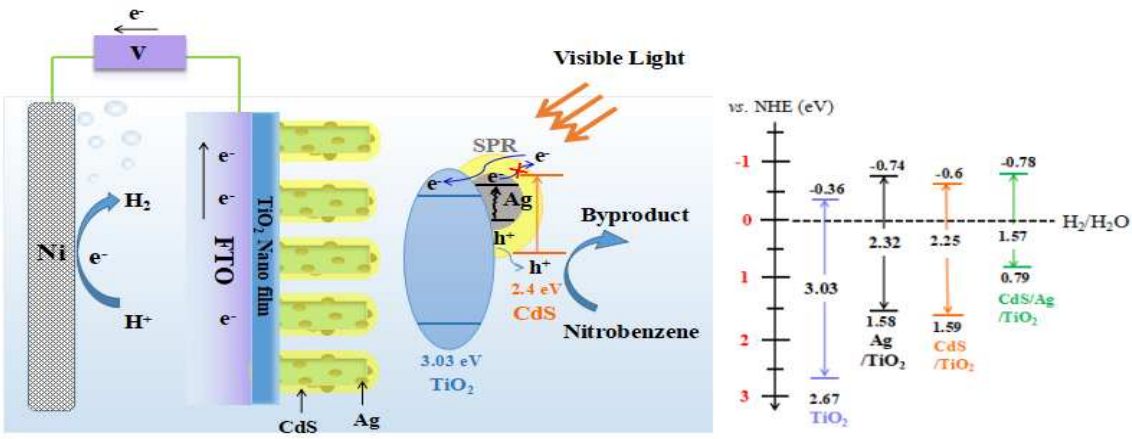

Scheme 2

Highlights:

- TiO_2 nanorods decorated with CdS and Ag^0 were prepared and anchored on to a FTO electrode.
- Simultaneous oxidation of nitrobenzene coupled with reduction of water to produced H_2.
- Ag particles loaded on the surface of TiO_2 nanoroads covered with CdS film uniformly.
- Photoconversion efficiencies for nitrobenzene degradation and H_2 production as high as 4.4%.
- The heterostructure of CdS/Ag/TiO_2-NRs electrode has solar energy conversion in PEC system.

Declaration of interests

☒ The authors declare that they have no known competing financial interests or personal relationships that could have appeared to influence the work reported in this paper.

☐The authors declare the following financial interests/personal relationships which may be considered as potential competing interests: